Effects of G-quadruplex ligands on the topology, stability, and immunostimulatory properties of G-quadruplex-based CpG oligodeoxynucleotides

Anh Thi Tram Tu[a, b, c, d], Kazuaki Hoshi [a], Yue Ma[e], Taiji Oyama[f], Satoko Suzuki[f], Kaori Tsukakoshi[e], Kazuo Nagasawa[e], Kazunori Ikebukuro[e], Tomohiko Yamazaki*[, a, b]

[a] Nanomedicine Group, Research Center for Functional Materials (RCFM), National Institute for Materials Science (NIMS), 1-2-1, Sengen, Tsukuba 305-0047, Japan

[b] Division of Life Science, Hokkaido University, Kita 10, Nishi 8, Kita-ku, Sapporo 060-0808, Japan

[c] Department of Magnetic and Biomedical Materials, Faculty of Materials Science, University of Science, Vietnam National University, 227 Nguyen Van Cu street, ward 4, district 5, Ho Chi Minh, 70000, Viet Nam

[d] Vietnam National University, Linh Trung ward, Thu Duc city, Ho Chi Minh City, 70000, Viet Nam

[e] Department of Biotechnology and Life Science, Tokyo University of Agriculture and Technology, 2-24-16, Naka-cho, Koganei 184-8588, Japan

[f] JASCO Corporation, 2967-5, Ishikawamachi, Hachioji, Tokyo 192-8537, Japan

*Corresponding author: YAMAZAKI.Tomohiko@nims.go.jp

ABSTRACT

We previously reported that the formation of G-quadruplex (G4) structures provides phosphodiester oligodeoxynucleotides containing unmethylated cytosine phosphate guanine (CpG ODNs) with higher nuclease resistance and cellular uptake, thereby increasing their immunostimulation efficiency through TLR9 activation. CpG ODNs forming G4 structures (G4 CpG ODNs) are thus potential vaccine adjuvants against infectious diseases. However, the G4 structure changes topology depending on the surrounding environment. Recently, G4 ligands, which are small molecules that bind to G4 ODNs with high affinity, were reported to improve the stability of G4. In this study, we propose to increase the stability and function of G4 CpG ODNs using G4 ligands. We show the effects of two G4 ligands, named L2H2-6OTD (L2H2) and L2G2-2M2EG-6OTD (L2G2), on the topology, stability, and immunostimulatory properties of a monomeric hybrid-type G4 CpG ODN containing CpG motifs in the central loop, named GD3. We found that L2H2 helps maintain the hybrid G4 topology of GD3 whereas L2G2 induces parallel G4 formation. Both G4 ligands increase the thermodynamic and nuclease stability of GD3. However, only GD3 associated with L2H2 binds efficiently to TLR9 and evokes a higher immune response from mouse macrophage-like RAW264 cells. GD3 associated with L2G2 does not bind efficiently to TLR9 and elicits lower cytokine production. Our results demonstrate that the potential to enhance immunostimulatory properties depends on the ability of G4 ligands to maintain and stabilize the hybrid G4 of GD3. We anticipate that our findings will facilitate the development of more effective G4 CpG ODN-based vaccine adjuvants against infectious diseases.

Keywords: guanine quadruplex, CpG oligodeoxynucleotide, toll-like receptor 9, phosphodiester backbone, G-quadruplex ligands

Unmethylated cytosine-phosphate-guanine (CpG) motifs are associated with pathogen infection because they are abundant in bacterial and viral DNA but rare in vertebrate DNA.[1] These CpG motifs are detected by Toll-like receptor 9 (TLR9), an innate immune receptor expressed in macrophages, B cells and dendritic cells (DCs).[2,3] Synthetic oligodeoxynucleotides containing unmethylated CpG motifs (CpG ODNs) trigger an immune response similar to that of bacterial DNA.[1] Therefore, in the absence of invading pathogens, intentional stimulation of the immune response by synthetic CpG ODNs provides a useful strategy in the development of vaccine adjuvants.[1] However, the therapeutic application of CpG ODNs is limited because they are rapidly cleared from the site of administration to the systemic circulation due to rapid degradation by nucleases.[4] Substitution of the oxygen of the phosphate group with sulfur creates a phosphorothioate (PT) ODN, which has higher resistance to nucleases,[4] but PT ODNs reportedly bind nonspecifically to proteins and form subcellular condensates, which may ultimately lead to diseases such as Alzheimer's.[5] In addition, PT ODNs causes thrombocytopenia, anemia, and neutropenia, raising concerns about the safety of PT ODNs. There is therefore need for nuclease-resistant CpG ODNs with natural phosphodiester (PD) backbones. We previously reported nuclease-resistant PD CpG ODNs which consist of two or three linked ODN2006_sequences, a well-known human TLR9 agonist.[6] More recently, we developed CpG ODNs that form guanine (G)-quadruplex structures (G4 CpG ODNs) and show increased nuclease resistance.[7,8]

G4 CpG ODN is a single-stranded ODN containing four tracts of three guanines and bearing immunostimulatory CpG motifs such as "GTCGTT" in the remaining (loop) regions of the sequence. The G-tracts in G4 CpG ODNs facilitate G-quadruplex (G4) formation, enhancing nuclease resistance and cellular uptake of CpG ODNs.[7] The CpG motifs play a key role in TLR9 activation and subsequent nuclear factor-κB (NF-κB) signaling pathways.[8] In addition, G4 CpG

ODNs potentiate the production of inflammatory cytokines, including interleukin (IL)-6 and IL-12 in mouse macrophage-like cells, human B cells, and human peripheral blood mononuclear cells (PBMCs).[7,8] These inflammatory cytokines promote innate immune responses and establish adaptive immunity,[9] suggesting that G4 CpG ODNs have potential as vaccine adjuvants against infectious diseases.

G4 is a non-canonical four-stranded DNA structure that forms spontaneously *in vivo* at the telomere of eukaryotic chromosomes or promoter regions and has a G-rich sequence.[10] G4 comprises stacking G-quartets, which are square planar arrangements of four guanines formed via Hoogsteen hydrogen bonds. A loop is any region connecting these G-quartets, and can be of various types such as propeller, diagonal or lateral. A diagonal loop connects two bases that are not base-paired in the same G-quartet. A propeller loop connects bases in the same groove of different G-quartets. Lateral loops form over a narrow groove or a wide groove and connect adjacent bases. Monovalent cations, including K^+ and Na^+ at the center, stabilize stacks of G-quartets by coordinating with the O6 of the guanine. G4s can be constructed from one strand (monomeric G4) or two, or four strands (multimeric G4). G4 exhibits diverse topologies, partly resulting from variations in strand orientation. Accordingly, parallel G4 structures have all four strands with the same 5'-3' polarity. Anti-parallel G4 contains two pairs of strands with reversed arrangement of 5'-3' polarity. Hybrid G4 has one strand oriented in the opposite direction to the other three strands.[11] Remarkably, the topology of G4 ODNs depends on the surrounding environment, including the nature and concentration of monovalent cations.[12] For example, Largy et al.[13] found that the G-rich DNA sequences 222 (d[$(G_3T_2)_3G_3$]) and 222T (d[$T(G_3T_2)_3G_3T$]) changed from anti-parallel to parallel G4 structures when the solution changed from sodium-rich

to potassium-rich.[13] These ODNs also underwent changes from 3-quartet parallel to 2-quartet anti-parallel structures when the concentration of K^+ was decreased below 1 mM.[13]

Small molecules called G4 ligands were recently developed to stabilize G4 structures by binding to G4 ODNs with high affinity.[14] G4 ligands commonly include an aromatic heterocyclic system to interact with G-quartets through π-π stacking and cationic groups to electrostatically interact with the loop or groove of G4.[14] We demonstrated the ability of the G4 ligands L2H2-6OTD[15], L2H2-2M2EA-6OTD and L2G2-2M2EG-6OTD to induce cation-independent G4 formation. These G4 ligands have structures based on telomestatin, a natural G4 ligand.[16] We also showed that L2G2-2M2EG-6OTD induces parallel G4 formation with high efficiency.[16] We regulated the topologies of G4-based aptamers using several G4 ligands, including L1H1-7OTD, L2H2-6OTD, Phen-DC3 and TmPyP4.[17] The G4-based aptamers T-SO530 and bivalent 3R02, which bind to α-synuclein (α-syn) oligomer and vascular endothelial growth factor (VEGF), respectively, showed enhanced binding ability to the target proteins in the presence of the G4 ligands.[17] In addition, Koirala et al. revealed higher mechanical and thermodynamic stability of the human telomeric sequence Tel-4G upon binding with G4 ligand pyridostatin.[18] Stronger forces required to unfold ligand-stabilizing G4 ODNs may additionally hinder the activity of DNA telomerases, which cause immortal replication in cancer cells.[10] A very recent study showed that L2H2 increases the thermodynamic stability and resistance to degradation of an endonuclease.[19]

Given the ability of G4 ligands to stabilize G4 ODNs, we expected that G4 ligands can stabilize G4 CpG ODNs and thus increase immunostimulatory activity. G4 ligands that can enhance the immune response to G4 CpG ODNs will facilitate the development of more effective vaccine adjuvants against infectious diseases. Therefore, in this study, we evaluated the effect of G4 ligands on the immunostimulatory properties of GD3, a monomeric G4 CpG ODN that we

previously reported.[8] We used the two G4 ligands L2H2-6OTD[15] and L2G2-2M2EG-6OTD[16] (hereafter referred to as L2H2 and L2G2, respectively). Both ligands contain a macrocyclic hexaoxazole to allow π-π stacking with G-quartets. In addition, L2H2 contains two symmetrical amino alkyl side chains whereas L2G2 bears four symmetrical guanidinylalkyl side chains, both of which bind to G4 grooves or loops. The topology, thermodynamic stability, nuclease resistance, intracellular uptake, and cytokine induction in mouse macrophage-like RAW264 cells of GD3 alone were compared with those of GD3 in complexes with L2H2 and L2G2, hereafter referred as GD3/L2H2 and GD3/L2G2, respectively.

RESULTS AND DISCUSSION

PD based G4 CpG ODNs address concerns regarding the adverse effects associated with PT-modified linear CpG ODNs as vaccine adjuvants. However, the G4 structure changes topology depending on the surrounding environment. In this study, we designed complexes of GD3, a G4 CpG ODN, and each of two G4 ligands, named L2H2 and L2G2 to examine whether the G4 topology can be stabilized and function of G4 CpG ODNs can be enhanced by G4 ligands. We discovered that the immunostimulatory efficiency of G4 CpG ODNs can be regulated by changing their physicochemical properties using G4 ligands.

Structural analysis of GD3 in complex with G4 ligands

GD3 is a monomeric G4 CpG ODN containing a G4 stem with three G-quartets connected by three loops: two external "TT" loops and one central loop containing three CpG motifs, "GTCGTT".[8] The sequence of GD3 is shown in **Figure 1A**. GD3 is a monomeric hybrid-type G4 CpG ODN with the highest immunostimulatory potential reported by our laboratory.[8] However, GD3 has a 22-base CpG motif in the central loop, resulting in a low T_m value of 41 °C. Increased

stability would facilitate further improvement of the immunostimulatory activity of GD3 and thus we choose GD3 as a model G4 CpG ODN in this study. The chemical structures of the two G4 ligands used in this study, L2H2 and L2G2, are shown in **Figure 1B i** and **1B ii**. Mixtures of GD3 and L2H2 or L2G2 were prepared at a molar ratio of ligand to ODN (R) of 4 because a previous study showed that the ligand-mediated topologies of G4 ODN are induced most clearly in the presence of four or more equivalents of ligand.[16]

Thermal difference spectra (TDS) were obtained to determine G4 formation. A negative peak at 295 nm in the TDS of GD3/L2H2 and GD3/L2G2 (**Fig. 1C i**) corresponds to denaturation of the G4 structure at high temperature, indicating that GD3/L2H2 and GD3/L2G2 form G4 structures.[20] Polyacrylamide gel electrophoresis (PAGE) was used to examine G4 molecularity, which defines the number of ODN molecules involved to the formation of a G4. PAGE analysis with running buffer containing K^+ (**Fig. 1C ii**) showed that GD3, GD3/L2H2, and GD3/L2G2 migrate faster than a linear ODN of the same length (ssODN38mer), indicating that GD3 in complexes with G4 ligands formed a monomeric G4 structure. GD3/L2G2 shows a smear instead of a distinct band because L2G2 changes slightly or mostly changes the GD3 structure, which results in a mixture of several structures that compete with each other during electrophoresis. Meanwhile, GD3/L2H2 shows a distinct band similar to that of GD3, because L2H2 does not induce changes in the GD3 structure.

To examine the ability of G4 ligands to induce G4 structures without monovalent cation, we conducted PAGE analysis with running buffer lacking K^+ (**Fig. 1C iii**) and observed that GD3 moved similar to the 35-base pair (bp) marker, indicating that GD3 did not retain the G4 structure without K^+. Furthermore, GD3/L2H2 and GD3/L2G2 showed two bands: one band that migrated the same as the 35-bp marker and another that migrated faster, suggesting that some ODN

molecules formed G4 structures induced by G4 ligands even in the absence of K^+. Size exclusion-high performance liquid chromatography was used to analyze the G4 molecularity of GD3 and GD3/G4 ligand complexes. **Figure S1** shows that a 38mer single-stranded linear ODN (ssCpG38mer) had a retention time of 12.72 min while GD3 had a longer retention time of 13.43 min, indicating that the hydrodynamic size of GD3 is smaller than that of its linear counterpart. GD3/L2H2 was retained in the column longer than ssCpG38mer and had a similar retention time as GD3, suggesting that it forms a monomeric G4. The chromatogram of GD3/L2G2 has a main peak at 13.72 min, revealing that GD3/L2G2 is more compact than GD3. Additionally, GD3/L2G2 shows an exceedingly small peak at 7.77 min, possibly attributed to the presence of a small amount of multimer G4 in GD3/L2G2. The HPLC analysis result of GD3/L2G2 did not show multiple peaks representing several competitive structures, unlike the result of the PAGE assay. This may be because HPLC analysis is based only on the variations in ODN size and is not influenced by the charge parameter that affects the results of the PAGE assay.

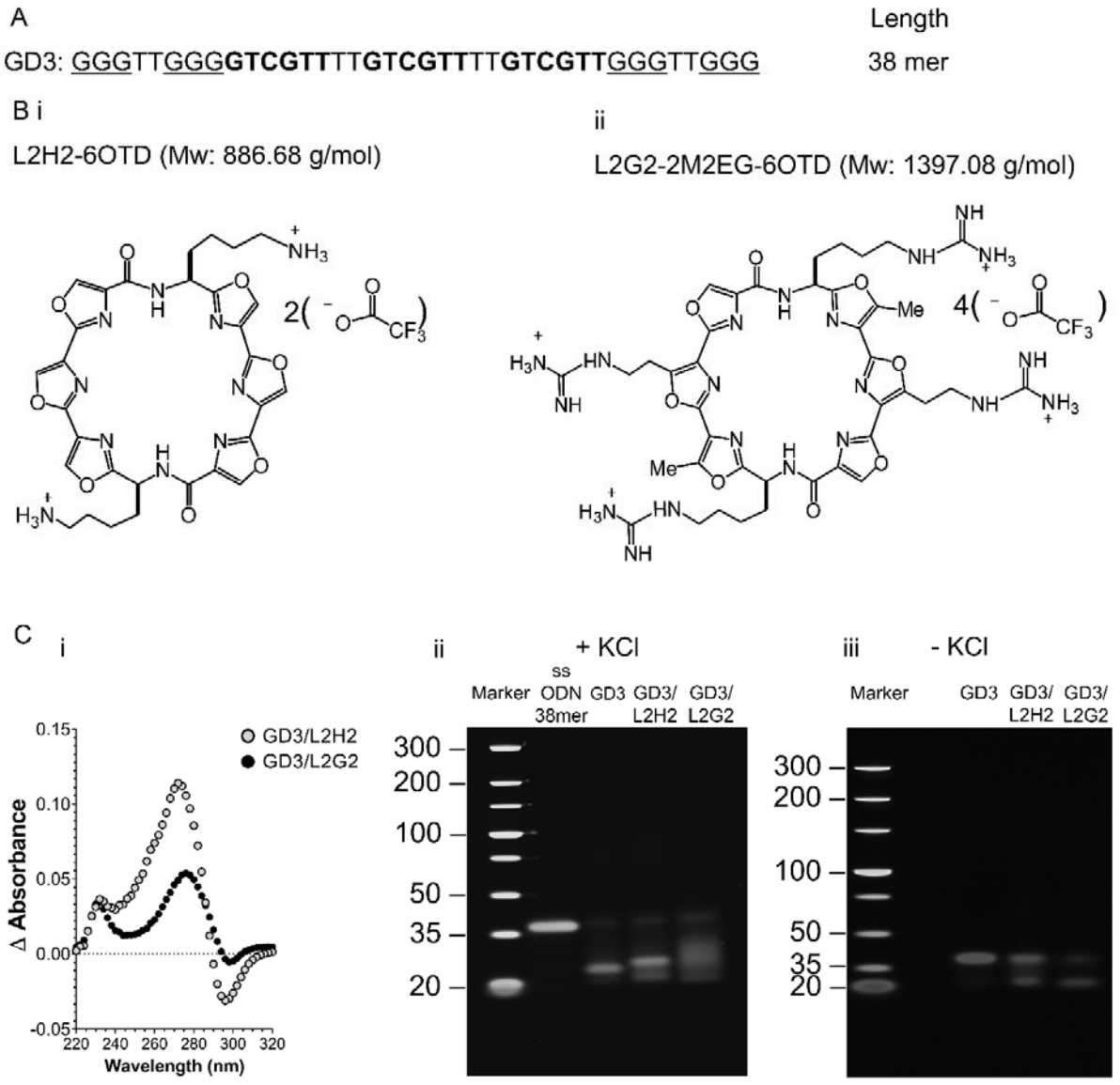

Figure 1 (A) Sequence of GD3. (B) Chemical structure of the G4 ligands (i) L2H2-6OTD (here referred to as L2H2)[15]; (ii) L2G2-2M2EG-6OTD (here referred to as L2G2)[16]. (C) Structural analysis of GD3 in a complex with G4 ligands at R = $n_{G4\text{-}ligand}$:n_{GD3} = 4. (i) Thermal difference spectra obtained by subtraction of the spectra obtained at 20 °C from those obtained at 90 °C. (ii) Polyacrylamide gel electrophoresis (PAGE) analysis in the presence of 4 mM KCl. (iii) PAGE analysis in gel and running buffer lacking KCl.

CD spectra were measured to examine the G4 topologies of the G4 CpG ODNs. The GD3 CD spectrum obtained at 25 °C showed a negative peak at 240 nm and a broad positive peak in the range of 260-290 nm (**Fig. 2A i**). The broad positive peak is due to overlap of a positive peak at around 280 nm, which corresponds to random structures of the long central loop, on two positive peaks at 260 and 295 nm, which correspond to the hybrid G4 stem.[8] As shown in **Figure 2A ii**, the spectrum of GD3/L2H2 has a negative peak at 240 nm and a broad positive peak ranging from 260–290 nm, which is akin to the CD spectrum of a hybrid G4. However, an absence of two distinct peaks at approximately 260 and 295 nm distinguished its shape from that of a typical hybrid G4. Meanwhile, the GD3/L2G2 CD spectrum (**Fig. 2A iii**) exhibited negative and positive peaks at 240 and 265 nm, respectively, suggesting a parallel G4 structure. Nevertheless, the bulge at approximately 280 nm does not infer the characteristic of a parallel G4 structure; thus, the attribution of its CD spectrum to the G4 topological group is also irrational. Consequently, a principal component analysis (PCA) of the CD spectra was conducted to clarify the topology of GD3/L2H2 and GD3/L2G2.[21]

The topology of the G4 structure has been used for analysis using the conventional rules-of-thumb. However, we also performed PCA to provide objective and quantitative information regarding the topological measurement prediction, which aided the interpretation of the CD spectra.[21] The PCA scores of GD3, GD3/L2H2 and GD3/L2G2 plotted on a PCA score plot are presented in **Figure 2B**. The PCA score of GD3 is in the 90% confidence limit of a hybrid structure, confirming that GD3 forms hybrid G4. The PCA score of GD3/L2H2 is out of this range but is close to the 80% confidence limit of the hybrid, indicating that GD3/L2H2 forms a structure similar to that of a hybrid G4 and that L2H2 only slightly changes the structure of GD3. The PCA score of GD3/L2G2 locates between the 80% confidence limits of parallel and hybrid structures but is

closer to the parallel structure, indicating that L2G2 may induce an equilibrium in which GD3 forms a structure analogous to a parallel structure and partially forms a hybrid structure. The dramatic change in the topology of GD3 from hybrid to parallel induced by L2G2 is consistent with a previous finding showing that L2G2 strongly regulates anti-parallel and hybrid to parallel type.[16] In summary, TDS, PAGE and SE-HPLC analysis showed that GD3 forms monomeric G4 structures in complexes with both G4 ligands. CD and PCA analyses of CD spectra revealed that GD3 and GD3/L2H2 form hybrid G4 structures whereas GD3/L2G2 is a mixture of mainly parallel and partly hybrid G4 structures.

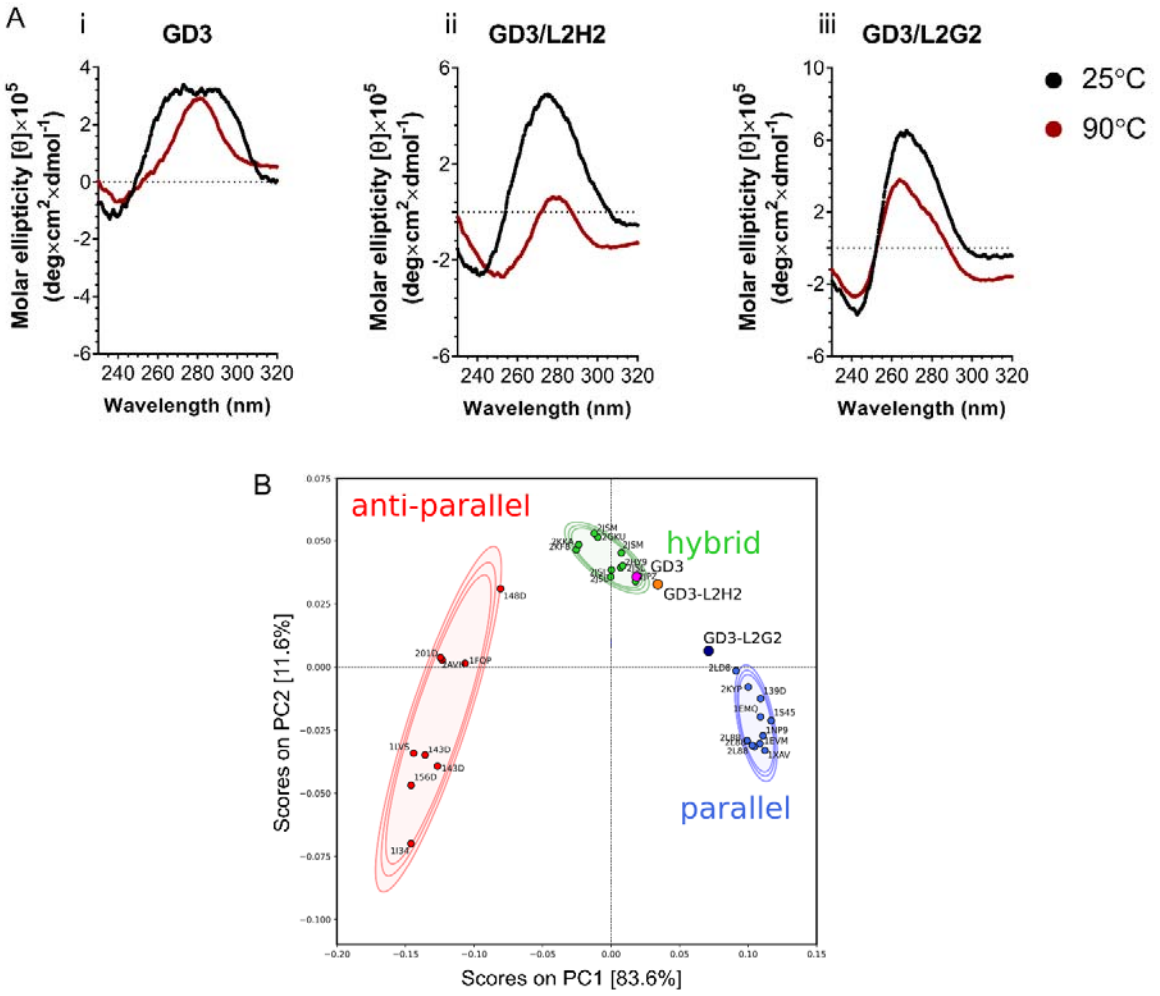

Figure 2 (A) Circular dichroism (CD) spectra at 25 °C and 90 °C of GD3 in complexes with G4 ligands at R = $n_{G4\text{-}ligand}$:n_{GD3} = 4. (i) GD3, (ii) GD3/L2H2, and (iii) GD3/L2G2. (B) The principal component analysis (PCA) scores of GD3, GD3/L2H2, and GD3/L2G2 are plotted in the PCA score plot. The ellipses indicate the 90%, 85%, and 80% confidence limits of each structure.

G4 ligands increase the thermodynamic stability of GD3

We elucidated the effects of the G4 ligands on the thermodynamic stability of GD3 by determining UV melting curves by recording UV absorbance at 295 nm during heating (**Fig. 3**). The melting temperatures of the G4 CpG ODNs are presented in **Table S2**. GD3/L2H2 showed a melting temperature at 77 °C whereas the melting curve of GD3/L2G2 did not show a transition in the temperature range of 20-90 °C, suggesting a melting temperature above 90 °C. The melting temperature of GD3 in complex with L2H2 and L2G2 increased compared with GD3 (T_m = 41 °C).[8] CD melting curves were conducted to examine the thermodynamic stability of G4 structures formed by GD3/L2H2 and GD3/L2G2. The spectra of GD3 and GD3/L2H2 obtained at 90 °C (**Fig. 2A i** and **Fig. 2A ii**) show a positive peak at 280 nm, corresponding to a random coiled structure, indicating that the G4 structure of GD3 and GD3/L2H2 is completely denatured at 90 °C. In contrast, the positive peak at 265 nm in the CD spectra of GD3/L2G2 is preserved at 90 °C (**Fig. 2A iii)**, suggesting that GD3/L2G2 remains as a parallel G4 structure. By subtracting the CD spectra at 90 °C from that at 25 °C, we discovered that the largest difference in molar ellipticity of GD3/L2H2 and GD3/L2G2 between low and high temperature occurred at wavelengths 265 nm and 270 nm, respectively, so we monitored the CD melting curves at these wavelengths (**Fig. S2**). The molar ellipticity of GD3/L2H2 (**Fig. S2A**) started to decrease at 70 °C, while that of GD3/L2G2 (**Fig. S2B**) was stable up to 90 °C, consistent with the UV melting curves. The UV and CD melting curves revealed that L2H2 and L2G2 increased the thermodynamic stability of GD3. The stabilizing abilities of these G4 ligands were observed in our previous study, which reported that L2H2 and L2G2 increase the melting temperature of the telomeric sequence telo21 by 19.1 and 25.3 °C, respectively.[16]

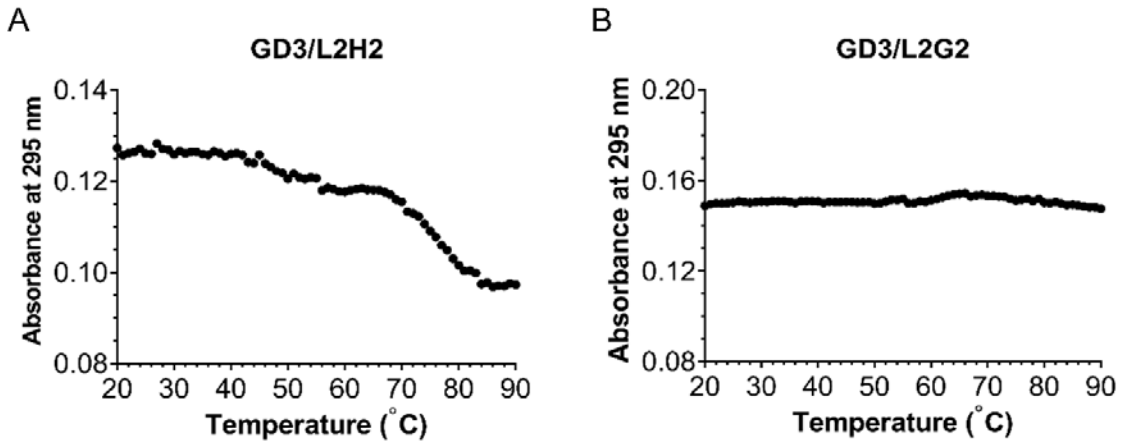

Figure 3 Ultraviolet (UV) melting curves of GD3 in complex with G4 ligands at R = $n_{G4\text{-ligand}}$:n_{GD3} = 4. UV absorbance at 295 nm was monitored during the heating of (A) GD3/L2H2 and (B) GD3/L2G2.

G4 ligands increase the stability of GD3 in serum

To clarify the effect of the G4 ligands on the nuclease resistance of GD3, we examined the stability of GD3, GD3/L2H2 and GD3/L2G2 in serum, which contains a mixture of endo- and exonucleases (**Fig. 4**). PAGE was used to evaluate the ODNs remaining after incubating in 18% fetal bovine serum for the indicated time (**Fig. 4A-C**). The ODNs showed two bands with different migration speeds. The upper bands with lower migration speeds correspond to molecules with random coiled structures while the lower bands with faster migration speeds correspond to molecules forming G4 structures. The contribution of G4-forming molecules to the amount of remaining ODNs was higher than that of random coiled molecules over the examined incubation time, indicating that the remaining ODNs were mainly in the G4 conformation. This result is compatible with the previous finding that G4 has higher nuclease resistance than linear structures.[8] An increase in the intensity of the upper band of GD3 after 1 h-incubation compared with 0 h-

incubation may be due to some fragmented molecules, generated during the first hour of incubation, that were unable to form G4 structures sufficiently stable to be observed on PAGE.

We attempted to evaluate the effect of G4 ligands on stabilizing the G4 structures by calculating the percentage of remaining G4-forming molecules relative to G4-forming molecules at the beginning of the incubation, based on the intensity of the lower bands (**Fig. 4D**). After 1 h of incubation, the amount of GD3, GD3/L2H2, and GD3/L2G2 remaining was 82%, 85%, and 96%, respectively. After 2-h incubation, 78% and 96% of GD3/L2H2 and GD3/L2G2, respectively, remained but only 67% of GD3. The difference in percentage of remaining ODN between GD3 alone and GD3 coordinating with G4 ligands were observed more clearly after 4 h of incubation, with a dramatic decrease in the percentage of remaining GD3 to 37%, whereas the amount of GD3/L2H2 and GD3/L2G2 remaining decreased to 68% and 84%, respectively. After 24 h, essentially no GD3 remained, whereas about 24% and 36%, respectively, of GD3/L2H2 and GD3/L2G2 remained. These results suggest that both G4 ligands increased the nuclease resistance of GD3, and that L2G2 was more effective than L2H2. This increased resistance of the G4 structure to nuclease activity is consistent with the observation that L2H2 decreases the susceptibility of HT24, a telomeric G4 ODN, to the endonuclease DNase 1.[19] G4 ligands increase the mechanical strength of G4 ODNs towards unfolding, possibly further preventing elongation by telomerases.[18] The reinforcement of G4 CpG ODNs by G4 ligands may make them more resistant to nuclease degradation.

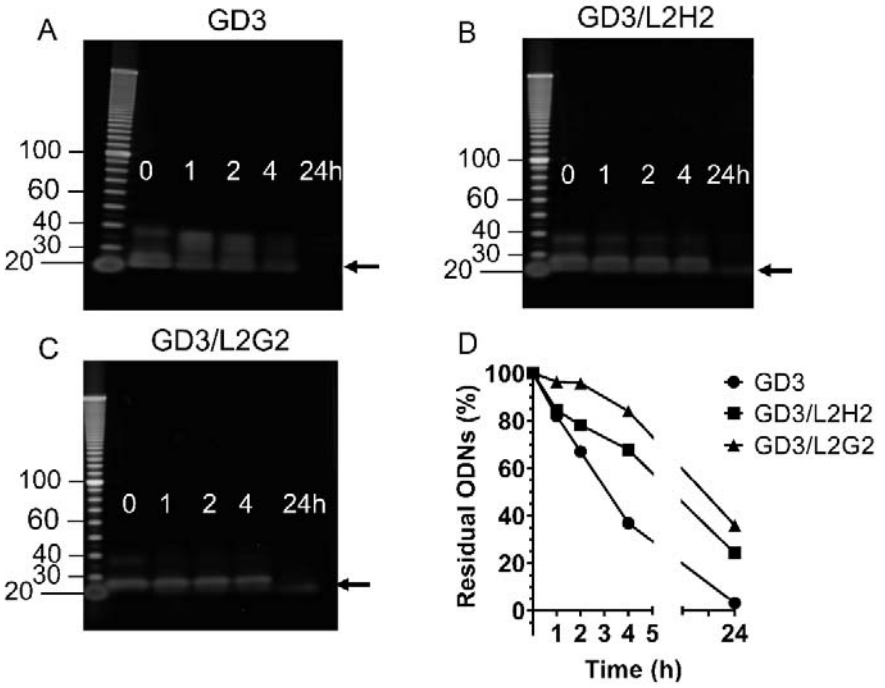

Figure 4 G4 ligands enhance nuclease resistance. PAGE analysis of (A) GD3, (B) GD3/L2H2, and (C) GD3/L2G2 after incubation for 1, 2, 4, and 24 h with 18% fetal bovine serum. The black arrows indicate the band corresponding to molecules forming G4. (D) Percentage of residual ODNs relative to the amount of ODN at the start of incubation.

Effects of G4 ligands on intracellular uptake of GD3

To evaluate the effects of the G4 ligands on the intracellular uptake of GD3, we examined the uptake of $GD3^{5'Cy5}$, $GD3^{5'Cy5}$/L2H2, $GD3^{5'Cy5}$/L2G2, and $2006\_PD^{5'Cy5}$ in RAW264 cells. The molar ratio of the G4 ligand to ODN in the complex examined for intracellular uptake is 4, which is similar to the ratio evaluated consequent to structural and biophysical analyses. $GD3^{5'Cy5}$ was reconstructed in D-PBS, and subsequently mixed with L2H2 and L2G2 solutions. The mixtures were incubated at 25 °C for 24 h prior to cell delivery. At 4 °C, receptor-mediated uptake was remarkably suppressed and thus we only observed ODN binding on the cell surface. At 37 °C,

receptor-mediated uptake was active and so the observed fluorescence signals represent cell-internalized ODNs. Histograms showing the fluorescence of cells treated with G4 CpG ODN at 4 °C and 37 °C are shown in **Figure S3 A** and **Figure S3 B**, respectively. The random CpG ODNs 2006_PD$^{5'Cy5}$ did not bind to the cell surface whereas the G4 CpG ODN GD3$^{5'Cy5}$ bound to the cell surface at 4 °C. Furthermore, the mean fluorescence intensity (MFI) values of cells treated with GD3$^{5'Cy5}$/L2G2 was 10 times higher than that of cells incubated with GD3 or GD3$^{5'Cy5}$/L2H2 (**Fig. 5**), suggesting that more GD3/L2G2 bound on the cell surface compared with GD3 or GD3/L2H2. This result is consistent with a previous study reporting that parallel G4 binds more strongly to cells than anti-parallel and hybrid G4.[22] At 37 °C, the MFI value of cells treated with GD3$^{5'Cy5}$/L2G2 was higher than that of cells incubated with GD3 (**Fig. 5**), implying that a larger amount GD3$^{5'Cy5}$/L2G2 was internalized. The cellular uptake of GD2/L2H2 was lower than that of GD3, possibly due to a small change in GD3 conformation induced by L2H2, as revealed by the PCA results (**Fig. 2B**).

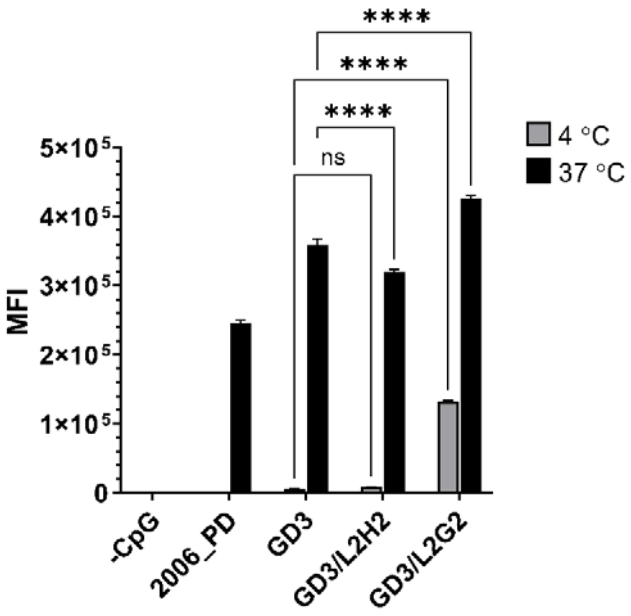

Figure 5 G4 ligands enhance cellular uptake of GD3. Uptake of Cy5-labeled CpG ODNs in RAW264 cells for 24 hours. Mean fluorescence intensity (MFI) of the cells incubated at 37 °C and 4 °C. RAW264 cells were incubated with 5 μM GD3$^{5'Cy5}$, GD3$^{5'Cy5}$/L2H2, GD3$^{5'Cy5}$/L2G2, or 2006_PD$^{5'Cy5}$ for 2 h. Data represent mean ± SD (n = 3). ****p < 0.0001, ns (not significantly different) p > 0.05 (one-way ANOVA, Tukey's multiple comparisons test for comparison with other groups).

Immunoprecipitation (IP) assay

An IP assay was conducted to examine the binding between TLR9 and GD3 alone and in complex with G4 ligands (**Fig. 6**). PAGE showed bands corresponding to GD3 and GD3/L2H2, suggesting that GD3 and GD3/L2H2 can bind to the ectodomain of mTLR9. We did not observe the GD3/L2G2 band in PAGE (**Fig. 6 i**), suggesting that GD3/L2G2 binds poorly to TLR9. In addition, we observed a comparable quantity of mouse TLR9Fc (mTLR9Fc) bound to protein-G-

conjugated beads in all samples, demonstrated by the similarity in band intensity upon sodium dodecyl sulfate (SDS)-PAGE (**Fig. 6 ii**).

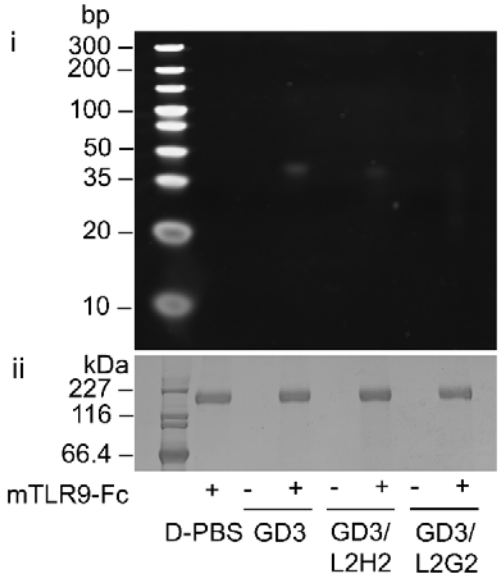

Figure 6 Immunoprecipitation binding assay of the binding between mouse TLR9 and GD3 or GD3 in the complex with G4 ligands at R = $n_{G4\text{-ligand}}$:n_{GD3} = 4. The assay was conducted at pH 6.5. GD3, GD3/L2H2, or GD3/L2G2 (250 pmol) was mixed with protein-G-conjugated beads with and without bound mTLR9Fc. The DNA bound to the beads was examined. (i) Polyacrylamide gel electrophoresis (PAGE) using a 10-20% polyacrylamide gel and 1× Tris-glycine running buffer and visualized using SYBR Gold staining. (ii) mTLR9Fc bound to protein-G-beads was detected by sodium dodecyl sulfate (SDS)-PAGE using a 15% polyacrylamide gel, 1× Tris-glycine-SDS running buffer, and Coomassie brilliant blue staining.

Immunostimulatory properties

To evaluate the effects of the G4 ligands on GD3-induced immunostimulatory activity, we examined the transcription and secretion of several cytokines by mouse macrophage-like RAW264 cells. First, the cytotoxicity of the ligand molecules was examined under the same condition as in

the immunostimulatory assay. The relative viability of RAW264 cells incubated with L2H2 and L2G2 was approximately 100%, which was comparable with that of the control, D-PBS. This indicates that the G4 ligands, L2H2 and L2G2, exhibited no toxicity (**Fig. S4**). **Figure 7Ai-iii** shows that GD3/L2H2 and GD3/L2G2, respectively induced higher and lower *IL-6*, *IL-12p40*, and *IL-10 mRNA* production in the cells compared with the expression induced by GD3. We also observed that the transcript level of IL-6 and IL-12p40 correlated with the protein secretion level in RAW264 cells (**Fig. 7Bi and ii**). A similar tendency was also observed for TNF-α secretion levels (**Fig. 7Biii**). The effects of L2H2 and L2G2 on IL-6, IL-12, IL-10 and TNF-α induction by GD3 were comparable, possibly because of the common NF-κB-mediated signaling pathway of these cytokines. **Figures 7Aiv and 7iv** show the relative interferon (IFN)-β mRNA and protein levels, respectively, in the RAW264 cells stimulated by GD3, GD3/L2H2, and GD3/L2G2. As shown in **Figure 7Aiv**, *IFN-β mRNA* expression levels induced by GD3, GD3/L2H2, and GD3/L2G2 stimulation are comparable and are at a low level. Further, we could not observe a GD3-mediated induction of IFN-β secretion, while a low level of secretion was induced by GD3/L2H2 and GD3/L2G2. The difference in the effect of G4 ligand on IFN-β induction of GD3 from other examined cytokines, may because IFN-β mediated by IRF-7, which is different with the transcription factor mediated inflammatory cytokine production.

To clarify the immunostimulatory effect of G4 ligands, we examined the activities of the G4 ligands alone and in complex with GD3_GpC, which is a GD3 variant with all the immunostimulatory CG dinucleotides inversed into non-immunostimulatory GC dinucleotides. As shown in **Figure S5 A-B**, L2H2 and L2G2 alone did not induce *IL-6*, and *IL-12 mRNA*. **Figure S5 C** exhibits that L2G2 slightly induced IFN-β. It is established that G4 ligands trigger the formation of micronuclei, which can be a source of cytoplasmic DNA.[23] This cytoplasmic DNA can activate

the stimulator of interferon genes (STING) via the action of the cytoplasmic DNA sensing machinery. This results in type I IFN (IFN-α/β) production.[23] Therefore, a modest level of *IFN-β* induction may be observed. Meanwhile, no *IFN-β* induction was observed following treatment with L2H2 alone (**Fig. S5 C)**, possibly because L2H2 has a lower affinity for DNA compared with L2G2, and consequently, has a lower potential for triggering micronuclei development. Although L2G2 alone induced IFN-β expression to a small extent (**Fig. S5C**), the expression induced by GD3/L2G2 was not higher, but comparable to that of GD3 (**Fig. 7Aiv**). These results suggest that L2G2 in complex with GD3 did not interfere with replication; thus, eliminating the probability of forming micronuclei. Furthermore, CG inversion completely abrogated the induction of all the cytokines in the GD3/L2G2 complex (**Fig. S6**), indicating that the immunostimulatory activity of the complex was strongly dependent on CG dinucleotides in GD3. This implies that L2H2 enhanced the function of GD3. This result suggests that the effect of G4 ligands on the topology of G4 CpG ODNs plays a critical role in TLR9 binding and the subsequent immunostimulatory activity of G4 CpG ODNs.

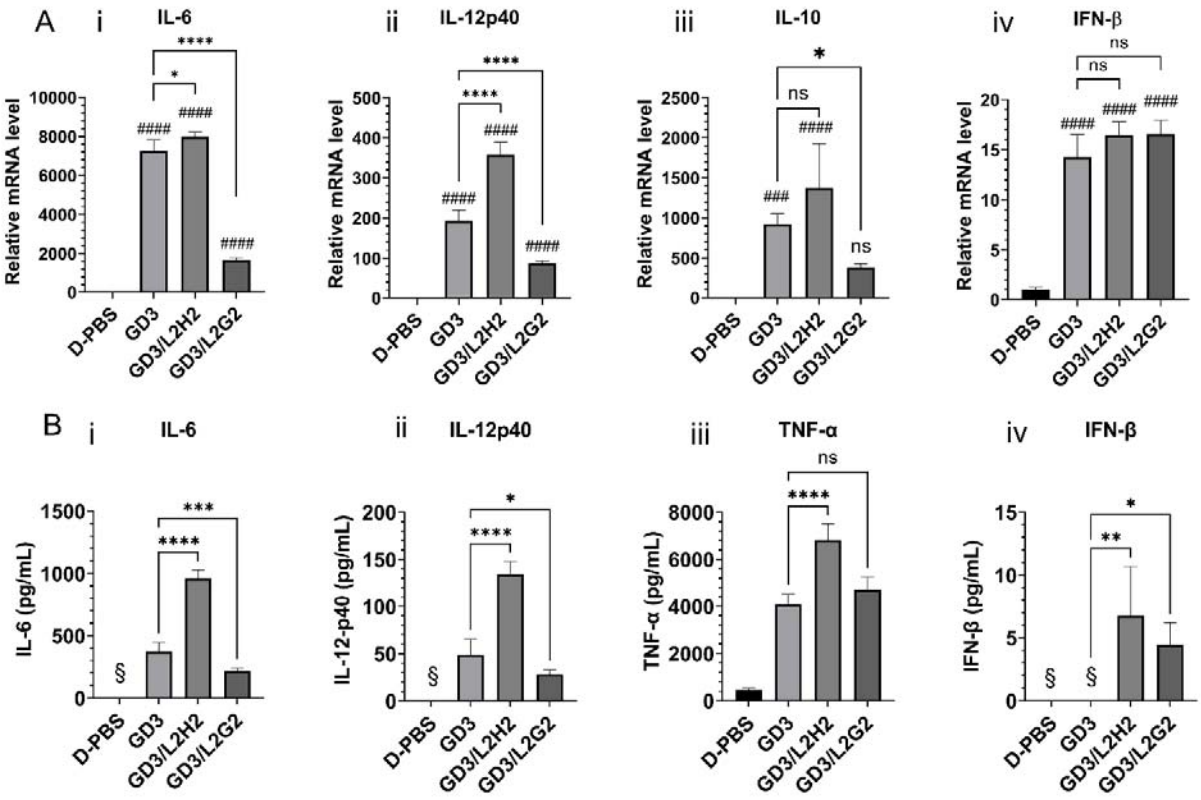

Figure 7 Cytokine induction in mouse macrophage-like RAW264 cells stimulated with GD3 and GD3 in complex with G4-ligands. (A) Relative mRNA levels of (i) *IL-6*, (ii) *IL-12p40*, (iii) *IL-10* and (iv) *IFN-β* expressed in the cells. The relative mRNA level compared to [D-PBS] was calculated. (B) The protein level of (i) IL-6, (ii) IL-12p40, (iii) TNF-α, and (iv) IFN-β secreted into the culture medium. Mouse macrophage-like RAW264 cells are incubated with 4 μM GD3, or GD3 in complex with /L2H2, or L2G2 at R = $n_{G4\text{-}ligand}$:n_{GD3} = 4 for 24 h. Data represent mean ± SD (n = 5). ****$p < 0.0001$, ***$p < 0.001$, *$p < 0.05$, ns (not significantly different) $p > 0.05$ (*, one-way ANOVA, Tukey's multiple comparisons test for comparison with other groups; #, Dunnett's multiple comparisons test for comparison with the D-PBS control group). §: lower detection limit (3.9 pg/mL, 7.8 pg/mL, 4 pg/mL for IL-6, IL-12p40, and IFN-β respectively).

An efficient immunostimulatory activity of CpG ODNs depends on three main factors, namely: nuclease resistance, cellular uptake, and binding efficiency to TLR9. Illustratively, high nuclease resistance enables the local ODN to gain an immunostimulatory potential greater than that of the required threshold for stimulation. In addition, a greater number of CpG motifs are protected from nuclease degradation and are thus available for TLR9 binding, which enhances and initiates TLR9 activation. Meanwhile, TLR9 is localized in intracellular compartments and endosomes; therefore, internalization of CpG ODNs is important for TLR9 activation. To induce immune responses via TLR9 activation, CpG ODNs must be taken up into the immune cells, in order to bind with the TLR9 in the endosomes. Furthermore, the binding affinity between TLR9 and CpG ODNs is directly proportional to TLR9 activation efficiency.[24] More efficient binding induces more effective TLR9 activation.[24]

The results of immunoprecipitation binding assay as shown in **Figure 6i** infer that GD3 and GD3/L2H2 can bind to the ectodomain of mTLR9. The band intensity of GD3/L2H2 was slightly lower than that of GD3 alone, indicating that the binding affinity between GD3/L2H2 and TLR9 is a bit lower than that of GD3 and TLR9. In addition, cellular uptake of GD3/L2H2 was slightly lower than that of GD3. Nevertheless, the serum stability of GD3/L2H2 is much higher than that of GD3. The high nuclease stability of GD3/L2H2 would compensate for its decreased cellular uptake efficiency and binding affinity. This might be the reason for the ability of GD3/L2H2 to stimulate higher cytokine induction than GD3 alone.

Despite its higher nuclease resistance and cellular uptake, GD3/L2G2 has lower cytokine induction compared with GD3. The IP assay showed that GD3/L2G2 does not bind to TLR9 efficiently, indicating that inefficient binding between GD3/L2G2 and TLR9 dramatically reduces the immunostimulatory properties. The G4 topology induced by G4 ligands may play a key role

in the binding between G4 CpG ODN and TLR9.[8] GD3/L2H2 forms hybrid G4 whereas GD3/L2G2 contains a large proportion of parallel G4. G4 ligand-induced topology can influence the binding between G4 CpG ODN and TLR9 in two ways. The first concerns charge distribution. In hybrid G4, the negative charges on the phosphate backbone are distributed throughout the structure. In contrast, in the parallel case, negative charges locate only at the side because the top and bottom of G4 are involved in π-π stacking interactions with G4 ligands.[16] This difference in charge distribution in G4 may lead to a difference in the binding mode between G4 ODNs and TLR9.[25] The binding mode between parallel GD3/L2G2 and TLR9 is likely less efficient than that between hybrid GD3/L2H2 and TLR9.

The second possibility relates to the flexibility of CpG motifs. The flexibility of CpG motifs in G4 structures impacts TLR9 recognition.[8] When GD3 changes the topology from hybrid to parallel G4, the degree of tension and deviation from planarity of the G-quartet change,[26] leading to a change in conformational mobility of G4 ODNs.[26] The conformation of the loop in the original hybrid structure is likely more flexible than the loop in the L2G2-induced parallel structure. The effects of G4 ligands on the structures and properties of GD3 are summarized in **Figure 8**.

Recently, we observed that apart from the hybrid, anti-parallel G4 also exhibits high immunostimulatory activity,[27] indicating that G4 topology (the sequence of glycosidic bond angles within the quadruplex stem),[28] does not directly influence the TLR9 activation efficiency. The change in topology consequently results in a change in the folding manner of the loops connecting the G-quartets and charge distribution, which may be the factors directly influencing TLR9 activation. Therefore, it is not as important to maintain the hybrid G4, but rather more the G4 topology, which facilitates CpG motifs easily interact with TLR9.

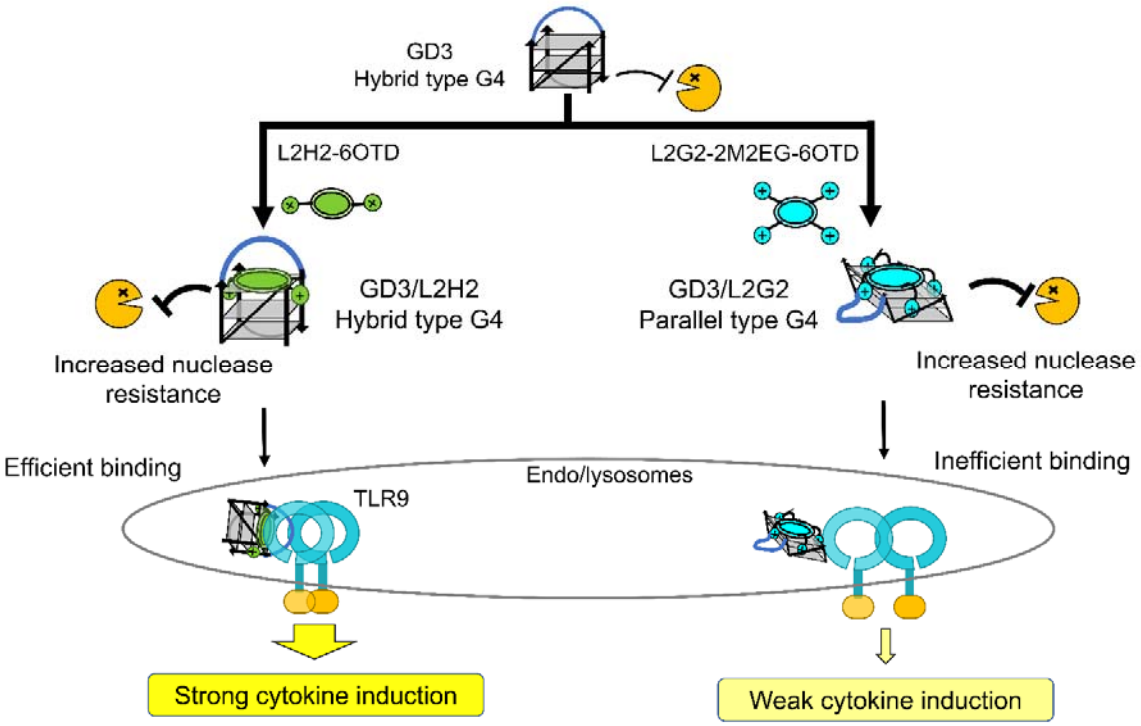

Figure 8 Schematic illustration of the effects of G4 ligands on G4 topology and the properties of G4 CpG ODNs. A hybrid-type monomeric G4 CpG ODN (GD3) was coordinated with the G4 ligands L2H2-6OTD (L2H2) and L2G2-2M2EG-6OTD (L2G2) (referred to as GD3/L2H2 and GD3/L2G2, respectively). L2H2 and L2G2 induce hybrid and parallel G4 structures of GD3, respectively. Both G4 ligands increase the nuclease stability of GD3. However, only GD3/L2H2 efficiently binds to TLR9 and triggers a strong immune response. GD3/L2G2 does not bind efficiently to TLR9, leading to lower cytokine production.

Aluminum salts (Alum) have been incorporated as adjuvants into vaccines for decades. Although alum can induce good Th2 antibody responses, it is less likely to trigger effective cellular immune (Th1) responses, which are important for perpetuating the autoimmune responses in cases requiring both the Th1 and Th2 for pathogen elimination.[29] Additionally, alum potentially results in local and systemic side effects, including sterile abscesses, eosinophilia, and

myofascitis[29]; thus, there is a need for the development of a safe and effective vaccine adjuvant. CpG ODN is an alternative vaccine adjuvant, however, the natural ODN, having an entire phosphodiester backbone, is susceptible to degradation by nucleases, which hinders its therapeutic application. Accordingly, phosphorothioate-modified ODN (PT ODN) has been investigated in clinical trials.[30] Consequentially, CpG 1018, a PT CpG ODN, has been approved as an adjuvant for hepatitis B vaccine (HEPLISAV-B) by the US Food and Drug Administration (FDA) in 2017. However, the high affinity of PT with various proteins in the body has raised concerns about adverse effects over the years, such as Alzheimer's disease.[5] Hence, recent research has focused on improving the nuclease resistance of CpG ODN without chemical modification. As reported in this work, only the phosphodiester CpG ODN and G4 binding ligand, which have been already established as therapeutic agents, were employed, enabling the system to acquire a major advantage regarding safety. Therefore, this study serves as an impactful resource for designing and establishing novel adjuvants.

In conclusion, we demonstrated that G4 ligands increased the thermodynamic stability and nuclease resistance of G4 CpG ODNs. The ability to enhance cytokine induction depends on the ability of G4 ligands to maintain and stabilize the structure of GD3. L2H2 is a potential G4 ligand for promoting the immunostimulatory efficiency of GD3 because it helps maintain the hybrid G4 topology, increases stability against nucleases, and helps conserve the binding between GD3 and TLR9. These findings may facilitate the development of a more effective vaccine adjuvant based on G4 CpG ODNs.

METHODS

Chemicals, oligodeoxynucleotides

L2H2-6OTD (**Fig. 1B i**) and L2G2-2M2EG-6OTD (**Fig. 1B ii**) were synthesized as described in Tera et al.[15] and Ma et al.[16], respectively. Their 1 mM stock solutions in DMSO were stored at -30 °C. GD3, which contains a natural phosphodiester backbone, was purchased as an HPLC-grade compound from Eurofins Genomic (Tokyo, Japan). The sequence of GD3 is presented in **Figure 1A**. A stock solution of GD3 was prepared in sterile purified water and stored at -30 °C.

Preparation of G4 CpG ODNs

Details of the preparation are presented elsewhere.[8] Briefly, GD3 stock solution was diluted with Dulbecco's phosphate-buffered saline (D-PBS, DS Pharma Biomedical, Osaka, Japan) and heated to 95 °C for 5 min, then cooled gradually to 30 °C for 30 min, followed by cooling to 4 °C. This solution of reconstructed GD3 was stored at 4 °C until use.

Ultraviolet (UV) melting curves and thermal difference spectra (TDS)

Details of measuring the UV melting curves and TDS analyses are presented in **Supplementary information**.

Polyacrylamide gel electrophoresis (PAGE)

GD3 was reconstructed in D-PBS. L2H2 and L2G2 stock solutions (10 mM) were diluted with sterile MiliQ water to a concentration of 1 mM. The reconstructed GD3 and G4 ligands were mixed to final concentrations of 10 μM and 40 μM, respectively (R = 4), then the mixtures were incubated at 25 °C for 24 h. Gel electrophoresis was conducted using 15% polyacrylamide gels

(ATTO, Tokyo, Japan) in 0.5× Tris-borate-EDTA (TBE) buffer (Takara Bio, Kusatsu, Japan) supplemented with 0 or 4 mM KCl. Details of the PAGE analysis are presented in **Supplementary information**.

Size exclusion-high performance liquid chromatography (SE-HPLC)

Sample preparation for SEC-HPLC is described in **Supplementary information**. SEC-HPLC analyses were performed at room temperature using a Shimadzu high-performance liquid chromatograph (C196-E061W Prominence, Kyoto, Japan) equipped with a Phenomenex (Bologna, Italy) Yarra SEC-2000 column (300 × 7.8 mm, 3 μm) and eluted with Dulbecco's phosphate-buffered saline (D-PBS, DS Pharma Biomedical, Osaka, Japan) containing 2.68 mM KCl, 137 mM NaCl, 1.47 mM KH_2PO_4 and 8.10 mM Na_2HPO_4. The flow rate was 0.6 mL/min and the eluate was monitored using a UV detector at 260 nm. For each analysis, 25 pmol ODN was injected onto the SEC column.

Circular dichroism (CD) spectroscopy

GD3 (20 μM) was reconstructed to form G4 structures in D-PBS. L2H2 and L2G2 stock solutions (10 mM) were diluted with sterile MiliQ water to a concentration of 1 mM. The reconstructed GD3 and the G4 ligands were mixed to final concentrations of 2 μM GD3 and 8 μM G4 ligand (R = 4). The mixtures were incubated at room temperature for 24 h before CD measurement. GD3 without G4 ligands was prepared by diluting 20 μM reconstructed GD3 with D-PBS to 2 μM. CD spectra were measured between 230 and 320 nm using the conditions previously reported.[8] Five scans were accumulated and averaged per presented spectrum.

Principal component analysis (PCA) of CD spectra was conducted to estimate their tertiary structures of GD3, GD3/L2H2 and GD3/L2G2. A library of 30 reference CD spectra of G4

structures (**Fig. S7A**) was used to create the PCA score plot shown in **Figure 2B**. Twenty two spectra of the reference CD spectrum of the G4-ODN library were previously published[21] and eight were obtained by our group. Comparison of the spectra of GD3, GD3/L2H2 and GD3/L2G2 with the average spectra of parallel, antiparallel and hybrid-type ODNs is shown in **Figure S7B**. The score plot was created using five principal components and processed by normalizing and centering the data.

Details of the CD melting curve measurements are given elsewhere.[8] CD melting measurements were performed at 265 nm and 270 nm for GD3/L2H2 and GD3/L2G2, respectively.

Intracellular uptake

GD3 and 2006_PD (5'-TC**GTCGTT**TT**GTCGTT**TT**GTCGTT**-3'), a well-known phosphodiester linear CpG ODN, were labeled at the 5' end with Cy5 ($GD3^{5'Cy5}$ and $2006\_PD^{5'Cy5}$). $GD3^{5'Cy5}$ was reconstructed in D-PBS. L2H2 and L2G2 stock solutions (10 mM) were diluted with sterile MiliQ water to a concentration of 1 mM. The reconstructed $GD3^{5'Cy5}$ and G4 ligands were mixed to final concentrations of 50 μM and 200 μM, respectively (R= 4), and the mixtures were incubated at 25 °C for 24 h. RAW264 cells were seeded in a 48-well plate at 2×10^5 cells per well and then incubated for 24 h at 37 °C in a humidified incubator with 5% CO_2. The culture medium was then replaced with 200 μL of Opti-MEM (Thermo Fisher Scientific) containing 5 μM $GD3^{5'Cy5}$, $GD3^{5'Cy5}$/L2H2, $GD3^{5'Cy5}$/L2G2 or $2006\_PD^{5'Cy5}$. After 2 h-incubation at 37 °C or 4 °C, the cells were washed with 500 μL phosphate-buffered saline (PBS; Wako Pure Chemical Corporation) twice and harvested. Flow cytometric analyses were then conducted using a flow cytometer (SP6800; Sony, Tokyo, Japan). Mean fluorescence intensity (MFI) was measured.

In addition, details of the stability in serum assay, cell culture, immunoprecipitation assay, cell viability assay, stimulation of RAW264 cells, reverse transcription/real-time quantitative-polymerase chain reaction (RT/RQ-PCR), enzyme-linked immunosorbent assay (ELISA), and statistical analysis are presented in **Supplementary information**.

ASSOCIATED CONTENT

Supporting Information

Supporting information including two parts: the experimental section and the figure and table section. The experimental section presents the method to obtain UV melting curves and thermal difference spectra, polyacrylamide gel electrophoresis; sample preparation for size exclusion-high performance liquid chromatography. In addition, this section presents cell culture process; assay to examine stability of ODN in serum and intracellular uptake; immunoprecipitation assay; and cell viability assay. The manner how we stimulate RAW264 cells; conduct reverse transcription/real-time quantitative-PCR, and ELISA, and do statistical analysis are also presented in the experimental section. The figure and table section contains the table presenting melting temperatures, the size exclusion-HPLC chromatograms of ODNs; circular dichroism melting profiles; histogram analysis of fluorescence intensity of RAW264 cells. Additionally, this section inculdes the bar graphs to show viability of RAW264; cytokine production of RAW264 cells. Furthermore, CD spectra of the library of 30 reference G-quadruplex ODNs; CD spectra of GD3, GD3/L2G2, and GD3/L2H2 in comparison with parallel, antiparallel, and hybrid reference spectra were also presented in this section.

AUTHOR INFORMATION

Corresponding author

*Nanomedicine group, Research Center for Functional Materials (RCFM), National Institute for Materials Science (NIMS) 1-2-1 Sengen, Tsukuba, Ibaraki, 305-0047 JAPAN. Phone number: +81-29-859-2345. Fax: +81-29-859-2449. Email: YAMAZAKI.Tomohiko@nims.go.jp

Author Contributions

A.T. carried out the experiment, analyzed data, and wrote the first draft of the manuscript. T.Y. contributed to study conception, design, and data interpretation. K.H. K.N., K.T, and K.I helped supervise the project. Y. M. synthesized the G4 ligands. T.O. and S.S. analyze the topology of oligonucleotide by principal component analysis. The manuscript was written through contributions of all authors. All authors have given approval to the final version of the manuscript to be published and agree to be accountable for all aspects of the work in ensuring that questions related to the accuracy or integrity of any part of the work are appropriately investigated and resolved.

Funding sources

This work was supported by the Japan Society for the Promotion of Science Kakenhi grant number (17KK0122, 18K04858, 21K19057).

Notes

The authors declare no competing financial interest.

ACKNOWLEDGEMENTS

We are deeply grateful to M. Takeuchi, A. Junko, A. Nagai, H. Sanematsu for their technical suggestions for the CD and UV analyses. This work was conducted at the NIMS Molecule and

Material Synthesis platform, supported by the Nanotechnology Platform Program of the Ministry of Education, Culture, Sports, Science and Technology (MEXT), Japan.

ABBREVIATIONS

ODNs, oligodeoxynucleotides; CpG, unmethylated cytosine-phosphate-guanine; G4, G-quadruplex; G4 CpG ODN, G-quadruplex-based CpG ODNs; IL-6, interleukin-6; IL-12, interleukin-12; TLR9, Toll-like receptor 9; pDCs, plasmacytoid dendritic cells; NF-κB, nuclear factor-κB; PBMCs, peripheral blood mononuclear cells; GAPDH, glyceraldehyde 3-phosphate dehydrogenase; ELISA, Enzyme-linked immunosorbent assay; RT/RQ-PCR, Reverse transcription/real-time quantitative-polymerase chain reaction; CD, Circular dichroism; UV, Ultraviolet; TDS, thermal difference spectra; PAGE, Polyacrylamide Gel Electrophoresis.

REFERENCES

1. Klinman, D. M. Immunotherapeutic uses of CpG oligodeoxynucleotides. *Nat. Rev. Immunol.* **4**, 249–259 (2004).

2. Suwarti, S., Yamazaki, T., Svetlana, C. & Hanagata, N. Recognition of CpG oligodeoxynucleotides by human Toll-like receptor 9 and subsequent cytokine induction. *Biochem. Biophys. Res. Commun.* **430**, 1234–1239 (2013).

3. Hanagata, N. CpG oligodeoxynucleotide nanomedicines for the prophylaxis or treatment of cancers, infectious diseases, and allergies. *Int. J. Nanomedicine* **12**, 515–531 (2017).

4. Mutwiri, G. K., Nichani, A. K., Babiuk, S. & Babiuk, L. A. Strategies for enhancing the immunostimulatory effects of CpG oligodeoxynucleotides. *J. Control. Release* **97**, 1–17 (2004).

5. The nucleotides that bind. *Nat. Biotechnol.* **38**, 1361 (2020).

6. Meng, W., Yamazaki, T., Nishida, Y. & Hanagata, N. Nuclease-resistant immunostimulatory phosphodiester CpG oligodeoxynucleotides as human Toll-like receptor 9 agonists. *BMC Biotechnol.* **11**, 88 (2011).

7. Hoshi, K. *et al.* G-quadruplex structure improves the immunostimulatory effects of cpg oligonucleotides. *Nucleic Acid Ther.* **29**, 224–229 (2019).

8. Tu, A. T. T., Hoshi, K., Ikebukuro, K., Hanagata, N. & Yamazaki, T. Monomeric G-Quadruplex-Based CpG Oligodeoxynucleotides as Potent Toll-Like Receptor 9 Agonists. *Biomacromolecules* **21**, 3644–3657 (2020).

9. Kaisho, T. & Akira, S. Toll-like receptor function and signaling. *J. Allergy Clin. Immunol.* **117**, 979–987 (2006).

10. Spiegel, J., Adhikari, S. & Balasubramanian, S. The Structure and Function of DNA G-Quadruplexes. *Trends Chem.* **2**, 123–136 (2020).

11. Kwok, C. K. & Merrick, C. J. G-Quadruplexes: Prediction, Characterization, and Biological Application. *Trends Biotechnol.* **35**, 997–1013 (2017).

12. Bochman, M. L., Paeschke, K. & Zakian, V. A. DNA secondary structures: Stability and function of G-quadruplex structures. *Nat. Rev. Genet.* **13**, 770–780 (2012).

13. Largy, E., Marchand, A., Amrane, S., Gabelica, V. & Mergny, J. L. Quadruplex Turncoats: Cation-Dependent Folding and Stability of Quadruplex-DNA Double Switches. *J. Am. Chem. Soc.* **138**, 2780–2792 (2016).

14. Sun, Z. Y., Wang, X. N., Cheng, S. Q., Su, X. X. & Ou, T. M. Developing novel G-

quadruplex ligands: From interaction with nucleic acids to interfering with nucleic acid–protein interaction. *Molecules* **24**, 396 (2019).

15. Tera, M. *et al.* Macrocyclic hexaoxazoles as sequence- and mode-selective G-quadruplex binders. *Angew. Chemie - Int. Ed.* **47**, 5557–5560 (2008).

16. Ma, Y. *et al.* Development of G-quadruplex ligands for selective induction of a parallel-type topology. *Org. Biomol. Chem.* **16**, 7375–7382 (2018).

17. Tsukakoshi, K. *et al.* Structural regulation by a G-quadruplex ligand increases binding abilities of G-quadruplex-forming aptamers. *Chem. Commun.* **52**, 12646–12649 (2016).

18. Koirala, D. *et al.* A single-molecule platform for investigation of interactions between G-quadruplexes and small-molecule ligands. *Nat. Chem.* **3**, 782–787 (2011).

19. Ishikawa, R. *et al.* Stabilization of telomeric G-quadruplex by ligand binding increases susceptibility to S1 nuclease. *Chem. Commun.* **57**, 7236–7239 (2021).

20. Mergny, J. L., Li, J., Lacroix, L., Amrane, S. & Chaires, J. B. Thermal difference spectra: A specific signature for nucleic acid structures. *Nucleic Acids Res.* **33**, 1–6 (2005).

21. del Villar-Guerra, R., Trent, J. O. & Chaires, J. B. G-quadruplex secondary structure obtained from circular dichroism spectroscopy. *Angew. Chemie - Int. Ed.* **57**, 7171–7175 (2018).

22. Chang, T. *et al.* General Cell-Binding Activity of Intramolecular G-Quadruplexes with Parallel Structure. *PLoS One* **8**, 1–10 (2013).

23. Miglietta, G., Russo, M., Duardo, R. C. & Capranico, G. G-quadruplex binders as cytostatic modulators of innate immune genes in cancer cells. *Nucleic Acids Res.* **49**, 6673–6686

(2021).

24. Pohar, J., Kužnik Krajnik, A., Jerala, R. & Benčina, M. Minimal Sequence Requirements for Oligodeoxyribonucleotides Activating Human TLR9. *J. Immunol.* **194**, 3901–3908 (2015).

25. Melisi, D. *et al.* Toll-like receptor 9 agonists for cancer therapy. *Biomedicines* **2**, 211–228 (2014).

26. Reshetnikov, R. V, Kopylov, A. M. & Golovin, A. V. Classification of G-Quadruplex DNA on the Basis of the Quadruplex Twist Angle and Planarity of G-Quartets. *Acta Naturae* **2**, 72–81 (2010).

27. Safitri, F. A. *et al.* Enhancement of the Immunostimulatory Effect of Phosphodiester CpG Oligodeoxynucleotides by an Antiparallel Guanine- Quadruplex Structural Scaffold. *Biomolecules* **11**, 1617 (2021).

28. Gibbs, S. & Miller, A. DNA quadruplex folding formalism – A tutorial on quadruplex topologies. *Methods* **64**, 28–35 (2013).

29. Petrovsky, N. & Aguilar, J. C. Vaccine adjuvants: Current state and future trends. *Immunol. Cell Biol.* **82**, 488–496 (2004).

30. Campbell, J. D. Vaccine Adjuvants. **1494**, 15–27 (2017).

GRAPHICAL TABLE OF CONTENTS